The robustness of an experimental procedure to predict the stability threshold speed in rotating machinery

B. Vervisch [1], **D. Ghyselinck** [1], **M. Monte** [1] **K. Stockman** [1], **M. Loccufier** [1]
[1] Ghent University, Department of Electrical Engineering, Systems and Automation
Graaf Karel de Goedelaan 5, B-8500, Kortrijk, Belgium
e-mail: **bramf.vervisch@ugent.be**

Abstract

High speed rotating machinery, with an operating speed above the first critical speed or above the first resonance frequency, is sensitive to instability. In this research, the robustness of an experimental procedure to predict the stability threshold speed in rotating machinery is discussed. The single degree of freedom model that is used in the experiments is discussed and the procedure is experimentally validated on a rotating damping setup. In this setup, the rotating damping is varied by means of tightening and loosening a flexible coupling. It is shown that it is possible to predict the stability threshold speed experimentally and that the rotor becomes unstable above this speed.

1 Introduction

Rotating damping instability is a phenomenon caused by internal damping in rotors that operate above the first critical speed or above the first resonance frequeny. Since this type of instability was reported in 1924 by Kimball [1], as a potential source of instabilities in high speed rotating machinery it has always been a design concern. Although hydrodynamic bearing instability, such as oil whirl and whip [2], was more important in those days rotating damping is still a major concern in the design phase of rotors. This is mainly because instability or self-excited vibration may not always be diagnosed as the main cause for breakdown or failure, but it is a root cause in many cases [3]. Especially under the influence of the aerospace industry, rotating damping research became more important [4,5]. In the 70s, stability problems caused by Space Shuttle main engines were a direct cause for a boost in the research efforts on rotating damping [6]. More recently, important contributions are reported toward the rotating damping instability with some experimental techniques. In [7] the potential of shrink fits to cause instability is described, in [8] the behaviour of shaft material and in [9,10] the influence on the frequency response functions [11,12]. However, there are some major problems in the experimental prediction of rotating damping. Rotating damping is not only a speed dependent phenomenon, causing speed dependent poles in the system, but it also results in asymmetric system matrices. Both the speed dependency and the asymmetry have a major influence on the experimental procedures. In a[13], the author proposes a procedure to estimate the decay rate of a rotor by measuring on a single location . By doing this, the stability threshold speed, or the speed at which the rotor becomes unstable, can be predicted experimentally. In this research, the robustness of the experimental method is tested. The rotating damping in a setup is changed by tightening and loosening a flexible coupling. Consequently, the friction between the coupling and the shaft is changed which results in a different rotating damping. It is shown that, for three situations, it is possible to predict the stability threshold speed. In section two, the single degree of freedom equivalent model used in the experimental procedure is discussed. Chapter three describes the rotating damping setup. In chapter four, the measurement procedure and the results are reported and discussed and the conclusions are summarized in section five.

2 The single degree of freedom equivalent

The experimental procedure that is validated in this research is described in [13]. In the following section, this procedure is described. First, the linear speed dependent model is derived which is decoupled into modal parameters. Because of the energy exhibited by rotatging damping a single degree of freedom model is proposed. This equivalent model is useful in an experimental procedure.

2.1 The linear speed dependent model

The class of rotating machinery discussed in this research are machines that show lateral flexibility within the operating conditions. The equations of motion contain a mass matrix $\mathbf{M}$, a damping matrix $\mathbf{C}$, and a stiffness matrix $\mathbf{K}$. Due to rotation, some of these properties change periodically in time resulting in time dependent matrices [14].

$$\mathbf{M}(t)\ddot{\mathbf{q}} + \mathbf{C}(t)\dot{\mathbf{q}} + \mathbf{K}(t)\mathbf{q} = \mathbf{f}(t), \quad \mathbf{q}(t), \mathbf{f}(t) \in \mathbb{R}^n \tag{1}$$

with n, the degrees of freedom. The vector of generalized coordinates, $\mathbf{q}$ is

$$\mathbf{q} = \begin{bmatrix} u_{xi} & \phi_{yi} & u_{xi+1} & \phi_{yi+1} & \dots & u_{yi} & \phi_{xi} & u_{yi+1} & \phi_{xi+1} & \dots \end{bmatrix}^\mathsf{T} \tag{2}$$

with u_{xi} translation in the x-direction, u_{yi} translation in the y-direction, ϕ_{yi} rotation around the x-axis and ϕ_{xi} rotation around the y-axis. In case of isotropic rotating elements, which accounts for the majority of rotating machinery, the time dependency can be narrowed down to a dependency upon the operating speed Ω

$$\mathbf{M}(\Omega)\ddot{\mathbf{q}} + \mathbf{C}(\Omega)\dot{\mathbf{q}} + \mathbf{K}(\Omega)\mathbf{q} = \mathbf{f}, \quad \mathbf{q}(t), \mathbf{f} \in \mathbb{R}^n \tag{3}$$

The most important effects that cause dependency upon the operating speed are the gyroscopic effect and the rotating damping. Both effects cause an asymmetry in the system, which can be written as

$$\begin{bmatrix} \mathbf{M} & \mathbf{0} \\ \mathbf{0} & \mathbf{M} \end{bmatrix} \ddot{\mathbf{q}} + \left(\begin{bmatrix} \mathbf{C}_n + \mathbf{C}_r & \mathbf{0} \\ \mathbf{0} & \mathbf{C}_n + \mathbf{C}_r \end{bmatrix} + \Omega \begin{bmatrix} \mathbf{0} & \mathbf{G} \\ \mathbf{-G} & \mathbf{0} \end{bmatrix} \right) \dot{\mathbf{q}} + \left(\begin{bmatrix} \mathbf{K} & \mathbf{0} \\ \mathbf{0} & \mathbf{K} \end{bmatrix} + \Omega \begin{bmatrix} \mathbf{0} & \mathbf{C}_r \\ \mathbf{-C}_r & \mathbf{0} \end{bmatrix} \right) \mathbf{q} = \mathbf{f} \tag{4}$$

with $\mathbf{G}$ and $\mathbf{C}_r$ respectively the gyroscopic matrix and the rotating damping matrix and $\mathbf{C}_n$ the non-rotating damping matrix. Due to the choice of the generalized coordinates in equation (2), both the gyroscopic effect and the rotating damping cause a coupling between the x- and y-coordinates.

2.2 Decoupling of the linear speed dependent model

By taking into account equation (2) and (4), the equations of motion can also be written as

$$\begin{cases} \mathbf{M}_x\ddot{\mathbf{q}}_x + (\mathbf{C}_{nx} + \mathbf{C}_{rx})\,\dot{\mathbf{q}}_x + \Omega\mathbf{G}_y\dot{\mathbf{q}}_y + \mathbf{K}_x\mathbf{q}_x + \Omega\mathbf{C}_{ry}\mathbf{q}_y = \mathbf{f}_x \\ \mathbf{M}_y\ddot{\mathbf{q}}_y + (\mathbf{C}_{ny} + \mathbf{C}_{ry})\,\dot{\mathbf{q}}_y - \Omega\mathbf{G}_x\dot{\mathbf{q}}_x + \mathbf{K}_y\mathbf{q}_y - \Omega\mathbf{C}_{rx}\mathbf{q}_x = \mathbf{f}_y \end{cases} \tag{5}$$

The advantage of this equation is that all matrices are symmetric. The mass, damping and stiffness matrices are half the size as in (4) and the coupling is achieved by the generalized coordinates $\mathbf{q}_x$ and $\mathbf{q}_y$ which correspond to the x- and y-coordinates in (2). Because, in stability analysis, the behaviour of the poles is important, it is interesting to describe the system in a single mode. Suppose that $\mathbf{X}$ is an undamped eigenvector of the first equation. These eigenvectors can be used to pre- and postmultiply the equations in (5)

$$\begin{cases} \mathbf{X}^\intercal \mathbf{M}_x \mathbf{X} \ddot{\mathbf{q}}_x + \mathbf{X}^\intercal \left(\mathbf{C}_{nx} + \mathbf{C}_{rx} \right) \mathbf{X} \dot{\mathbf{q}}_x + \Omega \mathbf{X}^\intercal \mathbf{G}_y \mathbf{X} \dot{\mathbf{q}}_y + \mathbf{X}^\intercal \mathbf{K}_x \mathbf{X} \mathbf{q}_x + \Omega \mathbf{X}^\intercal \mathbf{C}_{ry} \mathbf{X} \mathbf{q}_y = \mathbf{X}^\intercal \mathbf{f}_x \mathbf{X} \\ \mathbf{X}^\intercal \mathbf{M}_y \mathbf{X} \ddot{\mathbf{q}}_y + \mathbf{X}^\intercal \left(\mathbf{C}_{ny} + \mathbf{C}_{ry} \right) \mathbf{X} \dot{\mathbf{q}}_y - \Omega \mathbf{X}^\intercal \mathbf{G}_x \mathbf{X} \dot{\mathbf{q}}_x + \mathbf{X}^\intercal \mathbf{K}_y \mathbf{X} \mathbf{q}_y - \Omega \mathbf{X}^\intercal \mathbf{C}_{rx} \mathbf{X} \mathbf{q}_x = \mathbf{X}^\intercal \mathbf{f}_y \mathbf{X} \end{cases} \tag{6}$$

In case of light damping and an axisymmetrical system, the behaviour is described by

$$\begin{cases} \hat{m}\ddot{x} + (\hat{c}_n + \hat{c}_r)\dot{x} + \Omega \hat{g}\dot{y} + k\hat{x} + \Omega \hat{c}_r y = \hat{f}_x \\ \hat{m}\ddot{y} + (\hat{c}_n + \hat{c}_r)\dot{y} - \Omega \hat{g}\dot{x} + \hat{k}y - \Omega \hat{c}_r x = \hat{f}_y \end{cases} \tag{7}$$

$(\hat{\bullet})$ means that these are modal parameters. $\hat{m}$ and $\hat{k}$ are the modal mass and stiffness, $\hat{g}$ is the gyroscopic effect, $\hat{c}_n$ and $\hat{c}_r$ respectively representing the modal nonrotating and rotating damping and Ω the rotating speed. This system can be solved by assuming a harmonic solution of a free damped forward mode

$$x = r\mathrm{e}^{\sigma t}\cos(\omega t) \qquad ; \qquad y = r\mathrm{e}^{\sigma t}\sin(\omega t) \tag{8}$$

with σ the decay rate and ω the critical speed. Two new equations are derived by separating sine and cosine:

$$\begin{cases} \hat{m}\left(\sigma^2 - \omega^2\right) + (\hat{c}_n + \hat{c}_r)\sigma - \Omega \hat{g}\omega + \hat{k} = 0 \\ 2\hat{m}\omega\sigma + (\hat{c}_n + \hat{c}_r)\omega - \Omega g\sigma - \Omega \hat{c}_r = 0 \end{cases} \tag{9}$$

From the second equation σ is derived

$$\sigma = \frac{\Omega \hat{c}_r - (\hat{c}_n + \hat{c}_r)\omega}{2m\omega - \Omega \hat{g}} \tag{10}$$

This equation represents the decay rate of a single mode. In absence of the gyroscopic effect, ω is independent of the operating speed and $\hat{g}$ is zero. Therefore, the decay rate is an increasing straight line. At standstill σ is negative and it becomes positive at the stability threshold speed.

2.3 The energy of rotating damping

Although rotating damping appears as a stiffness term, the asymmetry has a particular effect on the energy distribution in the system. The force caused by rotating damping acts as a nonconservative force and causes a dissipation of energy. The work done by the displacement term or apparent stiffness term of the rotating damping is expressed as [3][15]

$$\begin{aligned} \mathrm{d}w = -\Omega \begin{bmatrix} 0 & c_r \\ -c_r & 0 \end{bmatrix} \begin{Bmatrix} x \\ y \end{Bmatrix} \begin{Bmatrix} \mathrm{d}x & \mathrm{d}y \end{Bmatrix} = \Omega \left(-c_r y \mathrm{d}x + c_r x \mathrm{d}y \right) \equiv f_x \mathrm{d}x + f_y \mathrm{d}y \\ \therefore \frac{\partial f_x}{\partial y} = -\Omega c_r \quad and \quad \frac{\partial f_y}{\partial x} = \Omega c_r \end{aligned} \tag{11}$$

Because $\partial f_x/\partial y \neq \partial f_y/\partial x$, dw is no exact differential, leading to a nonconservative force. This means that the rotating damping appearing as a stiffness term actually dissipates energy. Together with the regular damping, the sum of the nonconservative forces, P, of the rotating system can be written as

$$\begin{Bmatrix} P_x \\ P_y \end{Bmatrix} = -\begin{bmatrix} c_n + c_r & 0 \\ 0 & c_n + c_r \end{bmatrix} \begin{Bmatrix} \dot{x} \\ \dot{y} \end{Bmatrix} - \Omega \begin{bmatrix} 0 & c_r \\ -c_r & 0 \end{bmatrix} \begin{Bmatrix} x \\ y \end{Bmatrix} \tag{12}$$

If the rotor is operated at a speed Ω and whirling at ω, the expression of the whirling is a harmonic motion in x and y direction, $x = X\sin(\omega t + \phi_x)$ and $y = Y\sin(\omega t + \phi_y)$. The energy per cycle that is exchanged due to these forces can be expressed as

$$E_{cyc} = \oint P_x dx + P_y dy = \int_0^{2\pi/\omega} (P_x \dot{x} dt + P_y \dot{y} dt) \tag{13}$$

or

$$E_{cyc} = -\pi \left[\omega \left(c_n + c_r\right)\left(X^2 + Y^2\right) - 2\Omega XY \sin\left(\phi_x - \phi_y\right)\right] \tag{14}$$

This expression proofs that the appearance of rotating damping can lead to a positive energy per cycle or instablity. Whenever the whirling ω occurs in the same direction as the rotation Ω, which is called a forward mode, $\sin(\phi_x - \phi_y) > 0$. As Ω increases the influence of the second term in (14) is growing and instability can occur. For backward modes, $\sin(\phi_x - \phi_y) < 0$, the effect of the second term is always stabilizing.

2.4 The single degree of freedom model

The rotating damping, appearing as both a damping and a stiffness term entirely acts as a nonconservative force. Therefore, this physically is an apparent damping. Similarly, the gyroscopic effect is a conservative force, or an apparent mass. Combining these conclusions leads to an equivalent single degree of freedom model

$$\left(\hat{m} - \Omega\hat{g}_2\right)\ddot{x} + \left(\hat{c}_1 - \Omega\hat{c}_2\right)\dot{x} + \hat{k}x = 0 \tag{15}$$

in which the damping decreases as a function of the rotating speed. By proposing a harmonic solution

$$x = r\mathrm{e}^{\sigma t}\cos(\omega t) \tag{16}$$

this leads to

$$\begin{cases} -\hat{c}_2\Omega\sigma + \hat{m}(\sigma^2 - \omega^2) - \Omega\hat{g}_2(\sigma^2 - \omega^2) + \hat{c}_1\sigma + \hat{k} = 0 \\ \left(2\hat{m}\omega - 2\Omega\hat{g}_2\omega\right)\sigma + \hat{c}_1\omega + \Omega - \hat{c}_2\omega = 0 \end{cases} \tag{17}$$

and σ

$$\sigma = \frac{\Omega \hat{c}_2 \omega - \hat{c}_1 \omega}{2\hat{m}\omega - 2\Omega \hat{g}\omega} \tag{18}$$

by comparing (7) and (15), $\hat{c}_1$ and $\hat{c}_2$ are

$$\hat{c}_1 = \hat{c}_n + \hat{c}_r \tag{19}$$

$$\hat{c}_2 = \frac{\hat{c}_r}{\omega} \tag{20}$$

$$\hat{g}_2 = \frac{\hat{g}}{2\omega} \tag{21}$$

This equivalent system is convenient for the measurements. Classical techniques allow to estimate the parameters of this single degree of freedom model. The resulting model proofs that a simplified procedure can be used to estimate the stability threshold speed.

3 The rotating damping setup

The rotating damping setup has already been used in [13,16,17]. The key concept is a rotating shaft that is placed on bearings which are stiff in translation and rotation. The parts and properties are shown in Table 1. A schematic representation and a picture is shown in Figure 1 and 2. The shaft is excited during operation by means of an impact hammer and the response is measured by eddy current probes at different discrete rotating speeds. From these measurements, an approximation of the frequency response is made and used to estimate the poles. In this research, the main purpose is to change the rotating damping without changing the other properties of the rotor. The solution is found in the flexible coupling. By slightly adjusting the clearance in the left bearing, some tolerance is added to the coupling. By tightening or loosening of the screw, that fixes the coupling, the friction between the coupling and the shaft is altered.

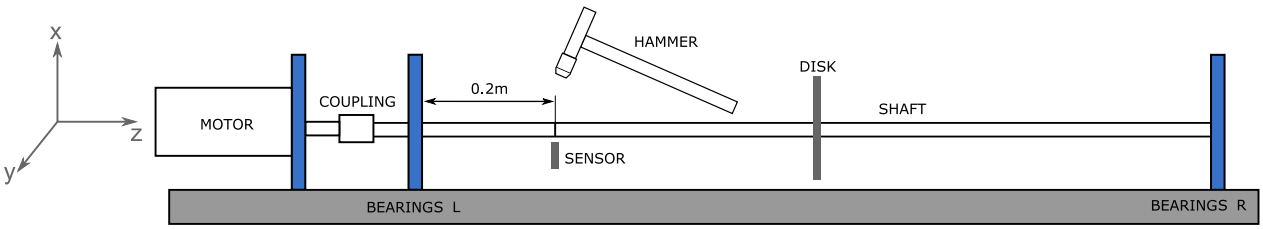

Figure 1: Schematic representation of the rotating damping setup

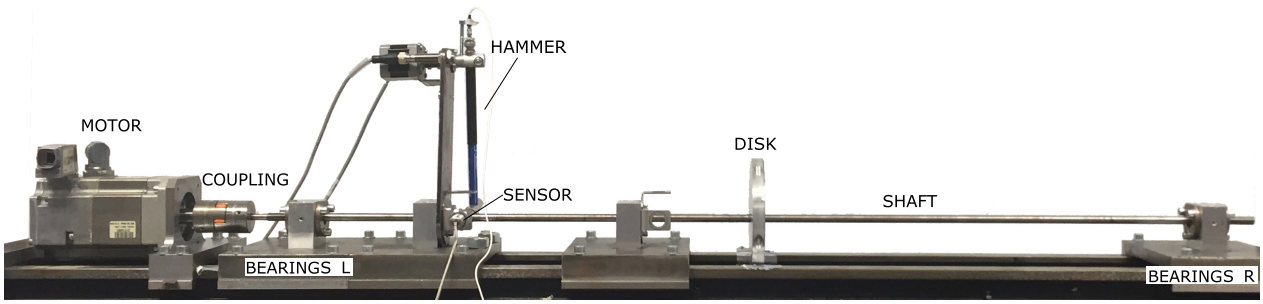

Figure 2: Picture of the rotating damping setup

Part	Type/properties
Shaft	Steel CF 53 - ∅ 0.01m - length 1.115 m
Disk	Aluminium - ∅ 0.15m - thickness 0.015 m
Bearings	FAG B7000-E-2RSD-T-P4S-UL - back to back - two at each side
Coupling	KTR-ROTEX 19
Motor	Siemens 1FK7042-5AK71-1UG0
EC probe	Monitran MTN/EP200
Impact hammer	Dytran 5800B2T

Table 1: Parts and properties of the rotating damping setup

4 Measurements

By exciting the shaft with the automated impact hammer and measuring the resulting displacement with the eddy current probes, a frequency response function is measured. This is performed at several operating speeds and in the three different situations of the coupling. The poles are extracted with a half power bandwidth method.

4.1 Measurement procedure

Figure 3 describes the measurement procedure that is used. At first the rotor is operated at a low speed. Standstill is not used because in practise, there is a small difference between the dynamic behaviour of the rotor at standstill and at a certain low speed. This effect is mainly caused by the motor. Second, the rotor is operated at an operating speed below the critical speed. At this operating speed, the rotor is stable and safe conditions are guaranteed. Consequently, by focussing on the first peak, the poles are extracted (Figure 4) and the decay rate plot is constructed. By gradually increasing the operating speed and keep monitoring the decay rate, a decay rate plot is obtained and the stability threshold speed is predicted.

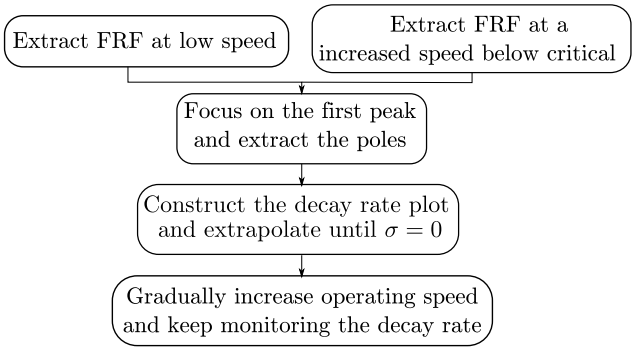

Figure 3: Flowchart of the measurement procedure

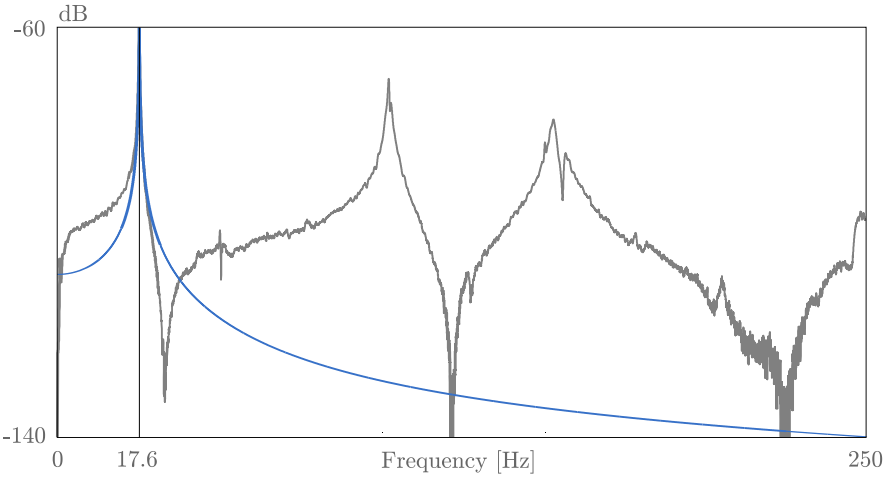

Figure 4: Approximation of the FRF by a single degree of freedom system

4.2 Results

The results for the decay rates are shown in Table 2 and plotted in Figure 5. On the graph, a linear fit is made for the low, medium and high damping. The measured critical speed occurs at 1056 rpm. As expected, the predicted stability threshold speed for the high damping is the lowest, 2430 rpm. The medium damping leads to 2647 rpm and the low damping leads to 5143 rpm. It is seen that there is some difference between the actual decay rates and the linear fit. This is mainly caused due unavoidable errors in the measurement. However, the predicted stability threshold speed can be validated. By increasing the speed until the stability threshold speed and monitoring the displacement, unstable behaviour can be detected. In Figure 6-8 the resulting instabilities are shown for low, medium and high damping. For each graph it is seen that there is a gradual increase of the magnitude. The measurement was stopped when the magnitude became to high and touched the chassis. It is seen that the dominant period equals 0.057s, which corresponds to 17,54 Hz or 1052 rpm, which is close the first critical speed. For the high damping, the rotor becomes unstable at 2400 rpm, slightly lower then the predicted stability threshold speed. For the medium and the low damping this is respectively 2600 rpm and 5100 rpm, also slightly lower. This small deviation ($< 2\%$) is caused by the slight errors on the decay rates.

Soft		Medium		Hard	
rpm	decay rate	rpm	decay rate	rpm	decay rate
100	-1,7	100	-1,375	100	-1,4
700	-1,15	700	-0,945	800	-0,93
1900	-0,4	1000	-0,8	2000	-0,65
		1900	-0,425	4000	-0,36
		2000	-0,22		
		2300	-0,27		

Table 2: Resulting decay rates at different operating speeds and low, medium and high damping

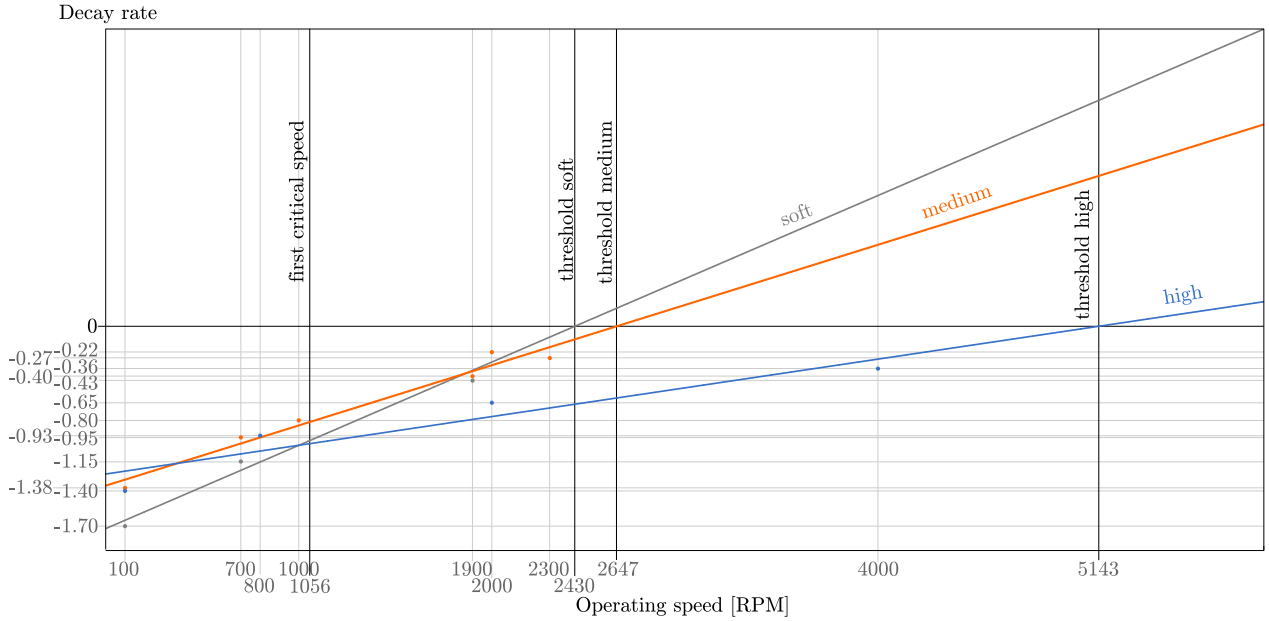

Figure 5: Comparison of the measured decay rate plot between low, medium and high damping

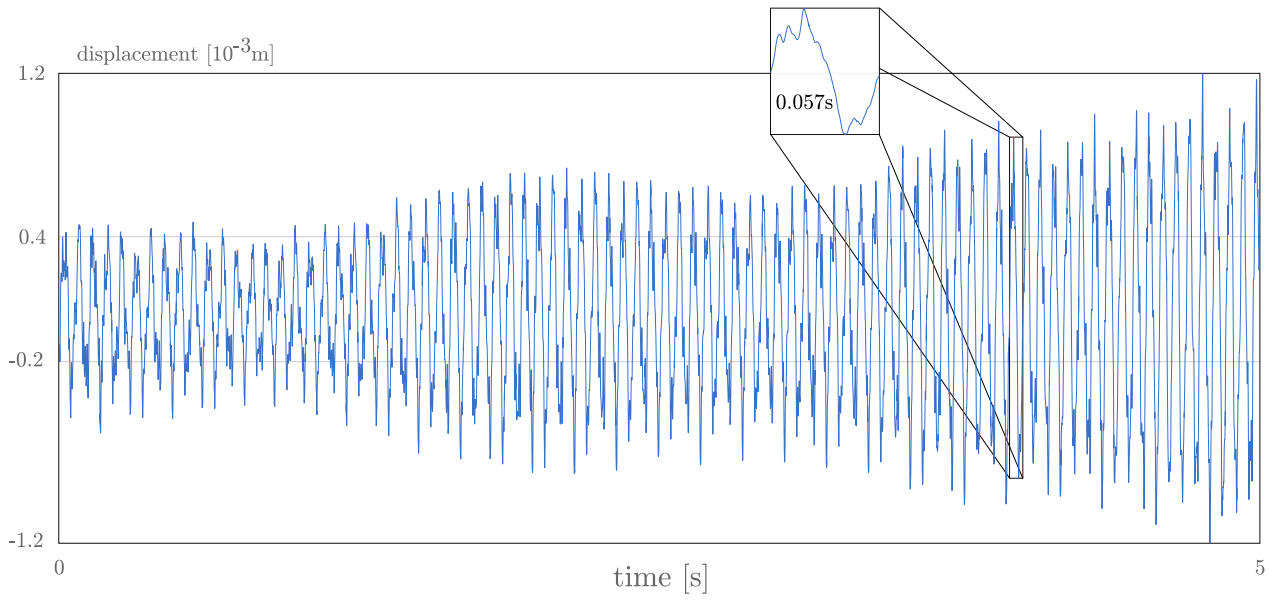

Figure 6: Unstable behaviour of the shaft for high damping at an operating speed of 2400 rpm

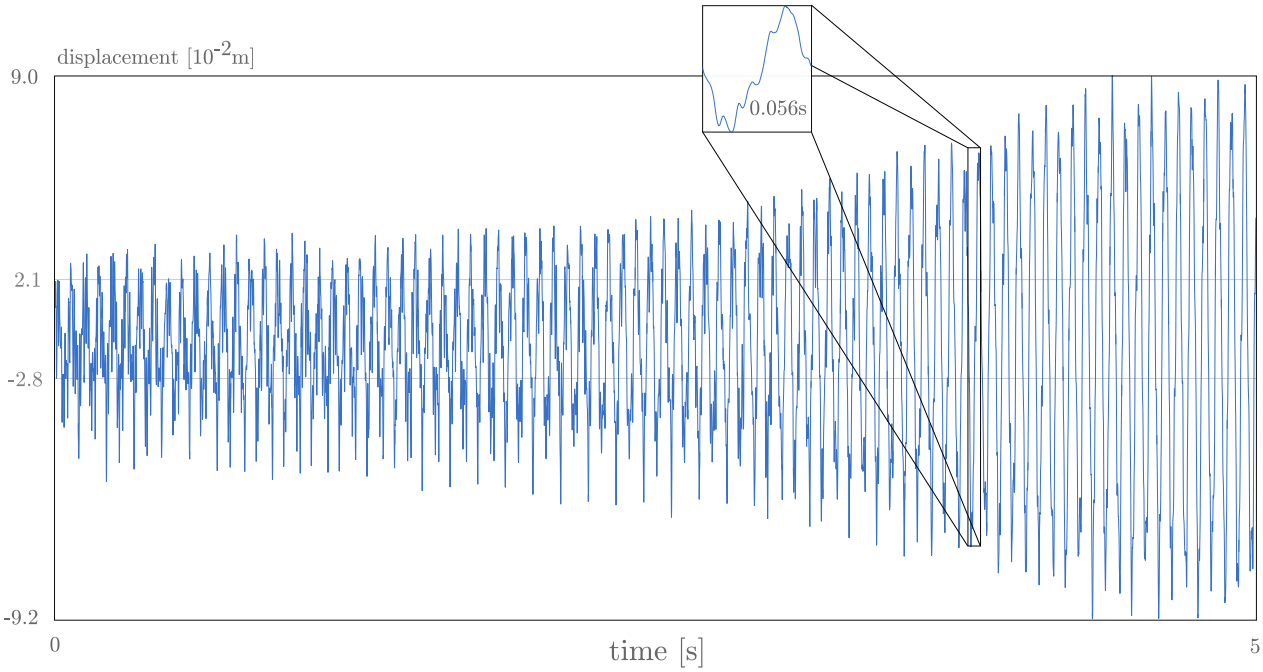

Figure 7: Unstable behaviour of the shaft for medium damping at an operating speed of 2600 rpm

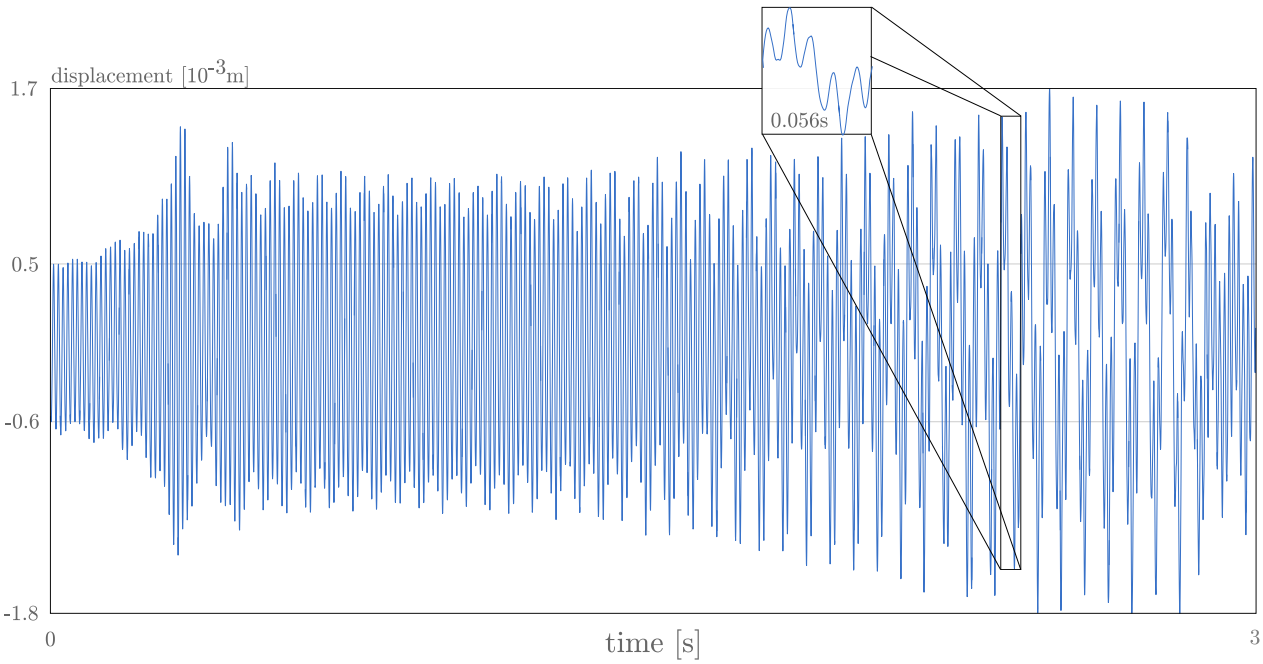

Figure 8: Unstable behaviour of the shaft for low damping at an operating speed of 5100 rpm

5 Conclusion

The present study was designed to determine the robustness of a procedure to predict the stability threshold speed in rotating machinery. The experimental procedure, described in a previous study, was tested for different values of rotating damping. It was expected that, for high rotating damping, the stability threshold speed would be low and for high rotating damping, it would be high.For three different situations: low, medium and high damping, the decay rate plot was extracted from measurements. The resulting plots confirm the

hypothesis as the high damping leads to the lowest predicted stability threshold speed and the low damping leads to the highest. By operating the rotor near this predicted stability threshold speed, it is shown that the rotor actually becomes unstable. From the decay rate plots it can be seen that the prediction of the stability threshold speed is highly dependent upon the errors on the decay rates at the different operating speeds. Future research might explore the possibility to increase the reliability of these measurements which would lead to an even higher accuracy of the predicted stability threshold speed.

References

[1] A. L. Kimball. *Internal friction theory of shaft whirling*. General Electric Review, 27:224–251, 1924.

[2] B. L. Newkirk, H. D. Taylor. *Shaft whipping due to oil action in journal bearings*. General Electric Review, 28(8):559–568, 1925.

[3] M. L. Adams. *Rotating machinery vibration: from analysis to troubleshooting*. CRC Press/Taylor & Francis, 2009.

[4] F. F. Ehrich. *Shaft Whirl Induced by Rotor Internal Damping*. Journal of Applied Mechanics, 31:279, 1964.

[5] E. J. Gunter, P. R. Trumpler. *The Influence of Internal Friction on the Stability of High Speed Rotors With Anisotropic Supports*. Journal of Engineering for Industry, 91(4):1105, nov 1969.

[6] D. W. Childs. *The Space Shuttle Main Engine High-Pressure Fuel Turbopump Rotordynamic Instability Problem*. Journal of Engineering for Power, 100(1):48, jan 1978.

[7] M. A. Kandil. *On Rotor Internal Damping Instability*. PhD thesis, Imperial College London, 2004.

[8] S. M. M. Jafri. *Shrink fit effects on rotordynamic stability: Experimental and theoretical study*. PhD thesis, Texas A&M University, 2007.

[9] E. Chatelet, O. Montagnier, G. Jacquet-richardet. *Dynamic Instability Analysis of Internally Damped Rotors. In Proceedings of GT2007*, number 1, pages 1–10, 2007.

[10] O. Montagnier, C. Hochard. *Dynamic instability of supercritical driveshafts mounted on dissipative supportsEffects of viscous and hysteretic internal damping*. Journal of Sound and Vibration, 305(3):378–400, aug 2007.

[11] M. Chouksey, S. V. Modak, J. K. Dutt. *Influence of rotor-shaft material damping on modal and directional frequency response characteristics. In Proceedings of ISMA 2010,* pages 1543–1558, 2010.

[12] M. Chouksey, J.K. Dutt, S.V. Modak. *Modal analysis of rotor-shaft system under the influence of rotor-shaft material damping and fluid film forces*. Mechanism and Machine Theory, 48:81–93, feb 2012.

[13] B. Vervisch, S. Derammelaere, K. Stockman, P. De Baets, M. Loccufier. *On the experimental prediction of the stability threshold speed caused by rotating damping*. Journal of Sound and Vibration, 375:63–75, aug 2016.

[14] I. Bucher, D. J. Ewins. *Modal analysis and testing of rotating structures*. Philosophical Transactions of the Royal Society A: Mathematical, Physical and Engineering Sciences, 359(1778):61–96, jan 2001.

[15] M. L. Adams, J. Padovan. *Insights into linearized rotor dynamics*. Journal of Sound and Vibration, 76(1):129–142, 1981.

[16] B. Vervisch, S. Derammelaere, K. Stockman, M. Loccufier. *Frequency response functions and modal parameters of a rotating system exhibiting rotating damping.* In *Proceedings of ISMA 2014 - International Conference on Noise and Vibration Engineering and USD 2014 - International Conference on Uncertainty in Structural Dynamics*, pages 2837–2850, 2014.

[17] B. Vervisch, K. Stockman, M. Loccufier. *Experimental Validation of Modal Parameters in Rotating Machinery.* In *IMAC XXXIII conference*, volume 6, pages 171–178, 2015.